Present-day upper-mantle architecture of the Alps: insights from data-driven dynamic modelling

Ajay Kumar[1], Mauro Cacace[1], Magdalena Scheck-Wenderoth[1,2], Hans-Jürgen Götze[3], Boris J.P. Kaus[4]

[1] GFZ, German Research Centre for Geosciences, Potsdam Germany

[2] Faculty of Georesources and Materials Engineering, RWTH Aachen University, Aachen, Germany

[3] Institute of Geosciences, Christian-Albrechts-University of Kiel, Kiel, Germany

[4] Institute of Geosciences, Johannes Gutenberg University of Mainz, Mainz, Germany

Corresponding author: Ajay Kumar (kumar@gfz-potsdam.de)

Keywords: Alps, Apennines, lithospheric architecture, slabs, seismicity

Key points:

- Statistical ensemble of S-wave tomography models is used to infer the LAB configuration and slab geometries in the Alps.
- The 3D upper-mantle architecture from the statistics reproduces first-order patterns in observed topography and GNSS vertical velocities.
- A shallow/attached slab in the Northern Apennines is consistent with the deep seismicity observed in this region.

Abstract

The dynamics of the Alps and surrounding regions is still not completely understood, partly because of a non-unique interpretation of its upper-mantle architecture. In this respect, it is unclear if interpreted slabs are consistent with the observed surface deformation and topography. We derive three-end member scenarios of lithospheric thickness and slab geometries by clustering available shear-wave tomography models into a statistical ensemble. We use these scenarios as input for geodynamic simulations and compare modelled topography, surface velocities and mantle flow to observations. We found that a slab detached beneath the Alps, but attached beneath the Northern Apennines captures first-order patterns in topography and vertical surface velocities and can provide a causative explanation for the observed seismicity.

Plain Language Summary

Present-day surface deformation, including earthquakes, plate motion, and mass (re)distribution, results from processes operating at the surface and in the inte-

rior of the Earth. Understanding these processes and their coupling is of utmost importance in the light of the hazard they pose to society. The Alps provide an excellent natural laboratory to understand such coupling. Here, we use seismic tomography models to constrain its upper-mantle architecture. We further use these models to quantify forces originating from the resolved architecture and their effects on the present-day surface deformation. The models can reproduce first-order patterns in the observed topography and vertical surface motions. We found a causative correlation between the presence of a shallow slab attached to the overlying lithosphere in the Northern Apennines and the seismicity in the region. Our results allow us to better understand the transfer of internal forces to the surface, thereby helping to quantify the present-day mechanical setup of the area.

Introduction

Geodetic observations by the Global Navigation Satellite Systems (GNSS) show that the Alpine mountains are uplifting while their forelands to the north and south are undergoing subsidence (Figure 1, Sternai et al., 2019; Pintori et al., 2022). Vertical uplift also varies along strike, with higher rates in the Western and Central Alps (~2-2.5 mm/yr) than in the Eastern Alps. Horizontal velocity from GNSS show ~2 mm/yr convergence between Adria and Europe in the Eastern Alps, being related to the counter-clockwise rotation of the Adria microplate with respect to Eurasia, while convergence is only minor, if not absent, in the Western Alps (Serpelloni et al., 2016). Active deformation, e.g. seismicity, in the area is also diverse, being restricted to upper-crustal depths in the Alps compared to whole crustal seismicity in their forelands (Figure 1). Intermediate-depth (>40 km) seismicity occurs only in the south, beneath the Northern Apennines. A combination of surface and/or mantle processes have been proposed to explain these observations, including: (i) isostatic response to the latest deglaciation, (ii) long-term erosion, (iii) crustal shortening, (iv) delamination of the European lithosphere, (v) detachment of the Western Alpine slab, and, (vi) mantle flow in the asthenosphere (Fox et al., 2015; Mey et al., 2016; Sternai et al., 2019). Quantifying the relative contribution of these processes to the present-day surface deformation is essential to understand the coupling between surface and mantle processes and the evolution of this complex orogen.

Mey et al. 2016 proposed that ~90% of rock uplift in the Alps could be due to crustal rebound following the Last Glacial Maximum (LGM), while mantle processes exert only a local influence (e.g., in the Rhone Valley and Eastern Alps). More recently, Sternai et al. 2019 critically revisited this hypothesis. They demon-

strated how deglaciation and erosion account for a relatively larger proportion of uplift in the Eastern Alps (30-60%) than in the Central and Western Alps (20-30%), and attributed the remaining uplift to other tectonic processes. This speculative contribution from tectonic processes stems from uncertainties in the upper-mantle (i.e., lithospheric mantle and asthenosphere) architecture. Recently, Spooner et al. 2019 developed the first gravimetric 3D density model of the crust in the Alps and their forelands. They found that a thicker crust beneath the Alps with intermediate average densities correlates with the observed surface uplift. They also noted that most Mw>6.0 earthquakes are located along boundaries between crustal domains of different average densities. Also, the long-term integrated strength of the crust and the lithosphere was found to correlate with the seismicity distribution (Spooner et al., 2022). Beneath the Alps, upper-crustal seismicity occurs within a weaker orogenic lithosphere, while weaker crustal domains are found preferentially around the stronger Adriatic microplate in the southern foreland. In the northern forelands, seismicity is also bound to weaker crustal areas which underwent extensive thinning beneath the Upper Rhine Graben (URG).

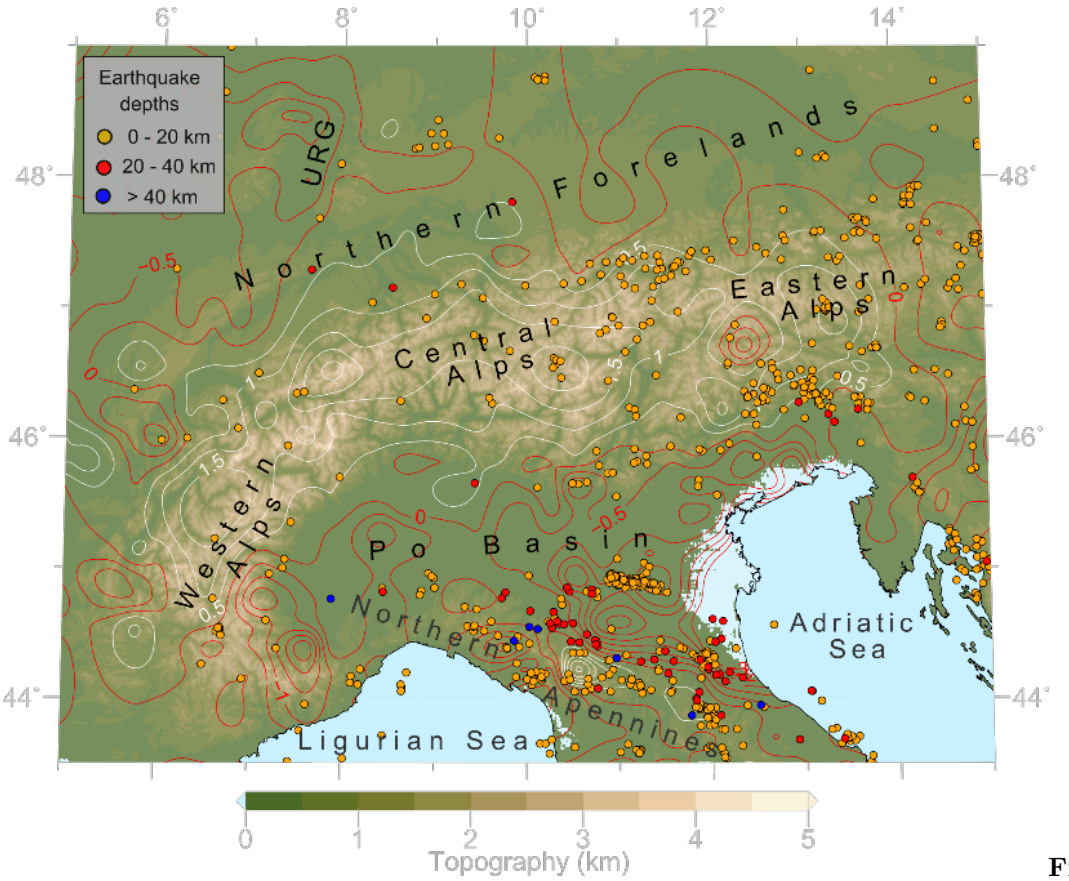

Figure 1: Topography map showing surface uplift (solid lines) and seismicity (circles) in the Alps and surrounding regions. Earthquakes are taken from the ISC reviewed bulletin (1964-2016, International Seismological Centre, https://doi.org/10.31905/D808B830) and are plotted with filled circles color-coded by depth (see legend). Vertical velocities from GNSS measurements (Sternai et al., 2019) are interpolated and contoured at a 0.5 mm/yr interval; white contours represent uplift, and red represents subsidence. Note that the 0 mm/yr contour is plotted in red.

These correlations indicate the importance of the lithospheric architecture in the localization of surface deformation within the Alpine region. However, the causality of these correlations remains subject to a proper quantification of the active driving forces. Forces within the Alpine lithosphere arise from horizontal plate motions, potential energy gradients due to present-day topography and lateral variations in density, and variations in surface loading conditions. Negative buoyancy from subducted lithospheric slabs within a weaker surrounding asthenosphere can generate flow and, therefore, stresses within and along the base of the lithosphere. Hence,

to quantify these forces and understand their contribution to the observed present-day surface deformation, it is crucial to determine the present-day 3D upper-mantle architecture.

Seismic tomography provides information to unravel the architecture of the upper-mantle. However, any interpretation of these models is non-unique (e.g., Foulger et al., 2013). For example, a recent interpretation of P-wave travel time tomography (Handy et al., 2021; Paffrath et al., 2021) suggests the presence of an European slab detached below the Western and Eastern Alps being locally attached to the lithosphere in the western Central Alps. In contrast, a surface-wave dispersion tomography model (El-Sharkawy et al., 2020) is consistent with slabs attached below most of the Central Alps. Kästle et al. 2020 compared all available regional high-resolution body-wave tomography models and concluded that slabs below the Alps differ significantly in their shapes and lengths. Differences in the interpretation of seismic tomography models arise from the choice of the reference model adopted and the relative velocity contrasts used to define velocity anomalies. Recent developments in the field of mineral physics and the availability of updated laboratory-derived pressure and temperature-dependent elastic properties can help to infer seismic velocities in terms of temperature and/or composition, thus providing a quantitative way to interpret tomography models (e.g., Cammarano et al., 2003; Goes et al., 2000; Priestley & McKenzie, 2006).

In this work, we use these additional constraints to determine the present-day upper-mantle architecture of the Alps and their forelands from available tomography models. We convert these models to temperature models to objectively determine the topography of the Lithosphere-Asthenosphere Boundary (LAB) and the geometry of slabs in the asthenosphere. These models are then used to compute the contribution to present-day deformation from buoyancy forces arising from the input configuration to add physical constraints to the present-day upper-mantle architecture.

Methods and data

Crust. The thickness of the crustal layers in the Alps and the surrounding regions is integrated from a 3D crustal model by Spooner et al. (2019). This model parameterized the crust into four layers: 1) unconsolidated sediments, 2) consolidated sediments, 3) upper-crust, and 4) lower-crust. In our study, we combine the sediments into one single layer and extend the model laterally to reduce potential boundary effects for the later geodynamic modelling stage by complementing it with the EuCrust-07 model (Tesauro et al., 2008), Figures 2a, b and c.

Upper-mantle. Shear-wave velocities (Vs) are more sensitive to variations in temperature than variations in composition (Kumar et al., 2020; Priestley & McKenzie, 2006). Thus, we use Vs tomography to map the temperature distribution in the mantle. We rely on four Vs tomography models, viz. CSEM (Fichtner et al., 2013, 2018), EU60 (Zhu et al., 2015), MeRe2020 (El-Sharkawy et al., 2020), and SL2013 (Schaeffer & Lebedev, 2013). CSEM and EU60 used three-component seismic waveform data to invert seismic velocities using full-waveform inversion and adjoint tomography methods. SL2013 is a global shear-wave velocity model inverted using multimode inversion of vertical component surface and S-waveforms. MeRe2020 is a Mediterranean scale model derived from an inversion of Rayleigh surface-wave phase velocity dispersion curves. To account for varying spatial resolutions of the tomography models, we interpolated all models to a common grid size of 20 km×20 km horizontally and 5 km in-depth, from 50 km to 300 km depth.

Conversion of seismic velocities to temperatures is highly non-linear because of the temperature and pressure dependence of elastic moduli, effects from anelasticity, and/or the presence of partial melts (Figure S1). To overcome this non-linearity, we pre-compute anharmonic Vs from the stable phase and mineral assemblages at upper-mantle pressure and temperature conditions. Stable phase and mineral assemblages are derived using a Gibbs free-energy minimization algorithm (Connolly, 2005, 2009). We use the augmented-modified version of Holland & Powell, 1998 thermodynamic database (Afonso et al., 2008; Afonso & Zlotnik, 2011) and depleted-mid-oceanic-ridge-basalt-mantle (DMM, Workman & Hart, 2005) as bulk composition in the upper-mantle. Pressure and temperature-dependent anharmonic Vs are corrected for anelastic attenuation and effects of partial melts using the parameters derived from laboratory experiments on olivine polycrystalline rocks (Jackson & Faul, 2010) and empirical relations for dry-peridotite solidus and liquidus (Hammond & Humphreys, 2000; Hirschmann, 2000; Winter, 2010; Afonso et al., 2016), respectively (Text S1).

The absolute Vs values from the tomography models are then projected onto the pre-computed look-up table of Vs using a lithostatic pressure profile derived from a thermo-chemical equivalent model of ak135 (Kennett & Engdahl, 1991; Kumar et al., 2020), thus providing a 3D distribution of temperature in the upper-mantle. We rely on a thermal definition of the LAB with a threshold temperature of 1300 °C as characteristic for the solidus of peridotite intersecting an average geotherm (Hirschmann, 2000). We use the 1300 °C isotherm to differentiate between lithospheric mantle, slabs, and asthenosphere. Regions corresponding to temperatures >1300 °C are defined as ambient asthenosphere. To distinguish between the lithospheric mantle and subducted slabs in the asthenosphere, we opted for a cut-off depth of 200 km; that is, if the 1300 °C isotherm lies above (below) this depth, then the portion of the mantle that is colder than 1300 °C is taken as lithospheric mantle (subducted slabs). The choice of this reference depth is justified by the observation that the Phanerozoic European lithosphere (LAB depth ~120 km, Griffin et al., 2009) can be as thick as 200 km beneath the Alps (e.g. Artemieva, 2019).

Buoyancy driven dynamic flow. To compute the deformation in response to the internal configuration, we solve the conservation of momentum and mass equations to calculate stresses, velocities, and topography using LaMEM (Text S2). The modelling domain is a 3-D Cartesian box with 96×96×128 grid points resulting in a resolution of ~13 km in E-W, ~17 km in N-S, and ~3 km along depth. Thicknesses of the crustal layers with respect to the digital elevation model, ETOPO1 (Amante & Eakins, 2009), are used such that we have an initial flat surface at 0 km which is modelled as an internal free surface (Crameri et al., 2012; Kaus et al., 2010). We adopt a free-slip boundary condition along the lateral edges and, a no-slip boundary condition along the base of the model (400 km). To further reduce potential lateral boundary effects, we extend the model by introducing a gap of 150 km width at the lateral sides and 100 km at the base of the model. We consider a first-order rheological structure where the lithosphere (i.e., sediments, upper-crust, lower-crust and lithospheric mantle) and slabs are stronger than the underlying asthenosphere (Table 1). Slabs are considered to be 70 kg/m^3 denser than the asthenosphere (Table 1). We also test the sensitivity of the model outcomes to variations in viscosity and density contrasts between the lithospheric mantle, slabs, and asthenosphere (Text S4 and Figures S9-S14). To investigate the dynamic effects of the internal buoyancy related to the upper-mantle configuration, we allow all models to obtain isostatic balance until a quasi-isostatic equilibrium is achieved (~0.27 Ma, Figure S2) and a return flow from the slabs is fully established without significantly deforming the slabs from their initial geometry (Figures 2 and 3).

Table 1: Physical properties of the different layers in the dynamic models. Densities in the crustal layers are according to Spooner et al. (2019).

Layer/Phase	**Density** (kg/m^3)	**Viscosity** ($Pa.s$)
Sticky-air	1	10^{18}
Sediments	2450	10^{22}
Upper-crust	2750	
Lower-crust	2950	
Lithospheric mantle	3370	
Slabs	3370	
Asthenosphere	3300	10^{20}

Results

Upper-mantle architecture. The geometry and depth extent of the slabs from each tomography model share some similarities in the Northern Apennines but differ significantly in the Alps (Figure S4). All regional tomography models (CSEM, EU60 and MeRe2020) depict an attached slab in the Northern Apennines with varying volume and position. In SL2013, a shallow slab is present from beneath the Northern Apennines to the Alps in the north. EU60 indicates

an attached slab all along the Eastern Alps, which is connected to attached slabs in the Western Alps and Northern Apennines. CSEM displays an attached slab at the transition between the Western and the Central Alps, similar to the interpretation of a recent P-wave tomography model (Handy et al., 2021). MeRe2020 shows a slab that is only locally attached to the lithosphere in the Central Alps.

Differences in slab geometries stem from the fact that the tomography models have varying magnitudes and spatial distributions of seismic velocities (Figure S5). Consequently, converted temperatures also differ, making it challenging to define a unique architecture of the LAB and slabs (Figures S4 and S5). Further, different methods, data and regularizations used in the inversion cause model-specific uncertainties. To objectively address such differences in the tomography models, we cluster them into a statistical ensemble, thereby assuming that these models sample a range of possible solutions. The statistical ensemble corresponds to the mean and standard deviation (*std*) of seismic velocities from all tomography models at each grid point. The mean of seismic velocities is clustered into a model (*mean* model hereafter*)*, whereas seismic velocities corresponding to the 67% confidence interval are clustered into two additional models (*mean-std* and *mean+std* hereafter*)*. The *mean-std* model represents an end-member scenario featuring no slabs beneath the Alps and the Northern Apennines (Figure 2d). The *mean+std* model is an end-member at the opposite spectrum where slabs are attached to the overlying lithosphere below the Alps and the Northern Apennines (Figure 2f). In the *mean* model, a slab is only attached to the overlying lithosphere beneath the Northern Apennines (Figure 2e).

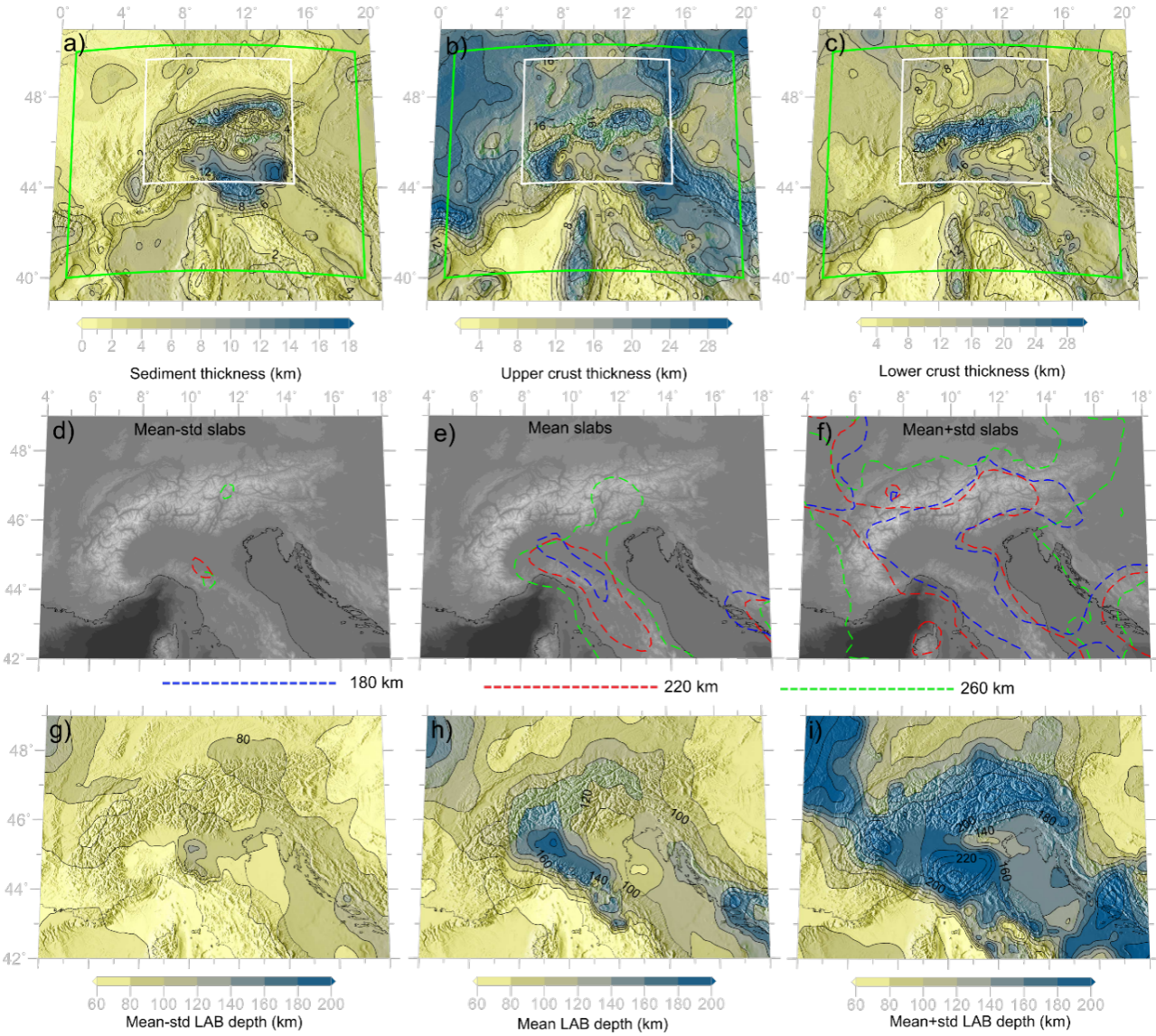

2: 3D crustal and upper-mantle architecture. Thickness of the a) sediments, b) upper-crust, and c) lower-crust. The white box in each panel marks the extent of the gravity constrained 3D crustal model, and the green box shows the extent of the region modelled in this study. Geometries of the slabs (d, e, and f) and LAB depths (g, h and i) for the statistical ensemble of tomography models. Color-coded dashed contours in panels d, e, and f delineate the slabs at 180 km, 220 km and 260 km depths.

Each model is also characterized by a varying LAB depth (Figures 2g, h, and i). All models show a thin lithosphere (~60-80 km) in the Ligurian Sea and

Pannonian Basin. The *mean-std* model results in a thinner lithosphere in the Alps and Northern Apennines. In the *mean* and *mean+std* models, the LAB depth is controlled by the presence of the slabs. Therefore, the *mean+std* model results in the thickest lithosphere beneath the Alps, Po Basin, and the Northern Apennines, where slabs are envisaged as attached to the lithosphere (Figures 2h and i). The presence of a thinner lithosphere in the northern forelands compared to the orogenic lithosphere in the Alps is a common feature of both the *mean* and *mean+std* models. In the following, we present the results of the geodynamic simulations for the statistical ensemble models. Simulations have also been carried out for the individual tomography models (Text S3 and Figures S4-S7).

Topography. In the absence of far-field tectonic forces, modelled topography is a function of the crust and lithosphere thickness and the geometry of the slabs, whether attached to or detached from the orogenic lithosphere. For the *mean-std* model, where no slabs are attached to the lithosphere, and the lithosphere is overly thin, the modelled topography reflects resolved crustal thickness variations (Figures 2c and 3a). It results in a negative topography along the present-day coastline in the Ligurian Sea and a positive topography in the Alps (~3-4 km), higher than in the northern forelands and Pannonian Basin. Along strike variations in crustal thickness in the Alps are also reflected in the modelled topography, being lower above the thinned crust in the Western Alps than in the Central and Eastern Alps. In the Northern Apennines, the model displays topography of similar magnitudes as in the Alps, which is inconsistent with observations (Figure 1). Despite similar magnitudes of crustal thickness beneath the Adriatic Sea and beneath the northern forelands (Figure 2c), the *mean*-std model results in positive topography all along the Northern Apennines to the Dinarides. The *mean* model features a lower topography in the Alps compared to the *mean-std,* still higher than that obtained in both forelands (Figure 3b). The lower topography in the Northern Apennines and Po Basin than the one obtained from the *mean-std* model can be explained by an attached slab in the Northern Apennines, which effectively pulls down the overlying lithosphere (Figure S3a). This gravitational effect is enhanced in the *mean+std* model (Figures 3c and S3b). As a result, the *mean+std* model does not produce any elevation gradient between the Alps and their forelands. The relatively high topography in the Adriatic Sea persists in the *mean+std* model, though of lower magnitudes due to a thicker lithosphere (Figure 2i).

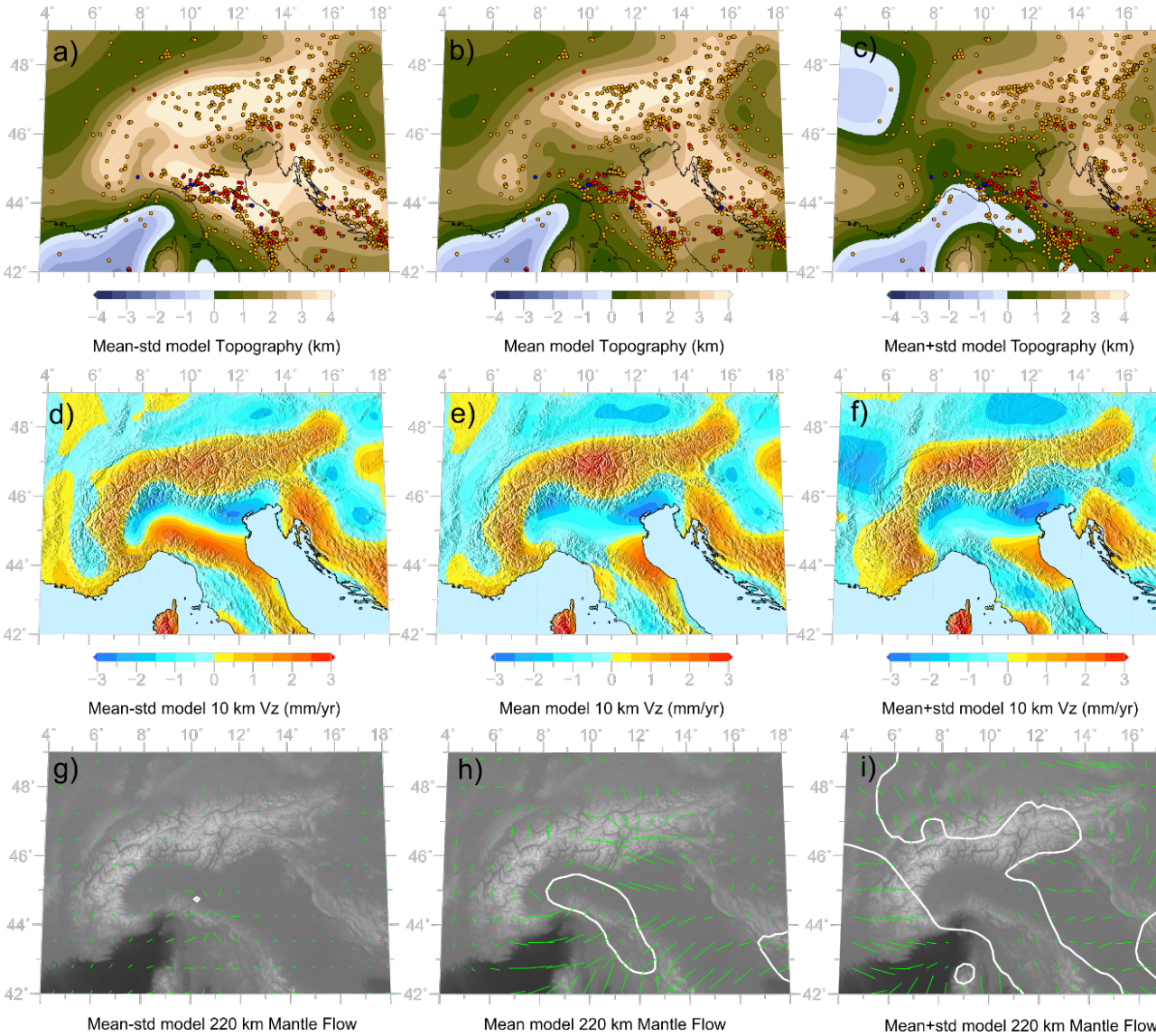

3: Modelled topography for a) *mean-std*, b) *mean*, and c) *mean+std* models. Seismicity color-coded for depth is same as in Figure 1. Modelled vertical velocities at 10 km depth for d) *mean-std*, e) *mean*, and f) *mean+std* models. Horizontal flow in the asthenosphere at a depth of 220 km for g) *mean-std*, h) *mean*, and i) *mean+std* models are plotted as green lines scaled by velocity magnitude. White lines in these last three panels indicate the contour of the slabs.

Surface vertical velocities. The geometries of the slabs also affect modelled vertical velocities. The *mean-std* model produces uplift in the Alps and subsidence

in the northern and southern forelands (Figure 3d). Subsidence in the Po Basin is limited by uplift in the Northern Apennines. In contrast, in the *mean* model, subsidence in the Po Basin continues to the south into the Northern Apennines (Figures 3e and S3c). The *mean+std* model, where slabs are attached all along the Alps and Northern Apennines, cannot reproduce the observed uplift in the Alps. Attached slabs to the thicker lithosphere lead instead to overall subsidence in the Po Basin, which continues to the north into the southern half of the Alps and to the south into the Northern Apennines (Figures 3f and S3d).

Mantle Flow. Horizontal flow in the asthenosphere also shows differences in terms of pattern and magnitude for the three scenarios (Figure 3g, h, and i). The *mean-std* model shows a less vigorous mantle flow than the *mean* and *mean+std* models due to the absence of slabs. In the *mean* model, we observe a rotation in mantle flow around the Western Alps due to a return flow generated by the attached slab in the Northern Apennines. This pattern is consistent with the shear-wave splitting (SKS) measurements that also show a rotation of the fast axis around the Western Alps (Barruol et al., 2011; Hein et al., 2021). In the *mean+std* model, such a rotation is hindered by the presence of an attached slab beneath the Alps. In the Central and Eastern Alps, the *mean* model displays an orogen-subparallel flow, which is not as coherent as observed in the SKS measurement. However, the *mean* model does reproduce the rotation in mantle flow at the transition from the Eastern Alps towards the Pannonian Basin, as observed in the SKS measurements.

Discussion and summary

Active subduction of oceanic lithosphere, attached to the overlying plate, is manifested in deep seismicity delineating the classical Benioff-Wadati zone. If the subducting lithosphere is in the process of tearing or breaking-off, it might show a concentration of intermediate-depth seismicity. Such a process is thought to be occurring in the Vrancea zone in the SE-Carpathians, where we observe a concentration of intermediate-depth seismicity and a positive seismic velocity anomaly (e.g., Wenzel et al., 2002). In the Alboran basin, a slab beneath the Betics mountains in Southern Iberia is also considered to be tearing/detaching, leading to the observed seismicity clustering (e.g., Heit et al., 2017; Mancilla et al., 2015). The preferred model for the slabs beneath the Alps portrays a detached slab in the Western and Eastern Alps (El-Sharkawy et al., 2020; Kästle et al., 2020; Lippitsch, 2003; Mark et al., 2021). Recent work indicated the possible presence of an attached slab in the western Central Alps (Handy et al., 2021). Lower-crustal seismicity in the European crust to the north of the Central Alps has been suggested to be driven by the transfer of stresses to the northern forelands from the retreat of a still attached slab (Kissling & Schlunegger, 2018; Singer et al., 2014). However, the absence of lower-crustal and intermediate-depth seismicity in the Alps rather indicates detached slabs all along the Alps. Our *mean* model, representing this scenario, can indeed reproduce the first-

order pattern in the observed topography and vertical velocities. An attached slab beneath the Central Alps will imply seismic deformation at lower-crustal depths or even at upper mantle depth levels. However, seismicity in the Alps is shown to be effectively bounded by the 450 °C isotherm within the upper crust (Spooner et al., 2020). These observations favor a detached slabs model, which can explain the presence of only upper-crustal seismicity beneath the Alps.

An attached shallow slab in the Northern Apennines is a robust feature in all regional tomography models. Our results suggest that such a configuration is also required to reproduce the present-day topography and subsidence rates observed in the Po Basin and Northern Apennines. An attached slab is also consistent with the observed intermediate-depth seismicity (e.g., Chiarabba et al., 2005), with earthquakes occurring at depths where we would otherwise expect rocks to behave aseismically.

None of the models in the statistical ensemble is able to reconcile the observed counter-clockwise rotation of Adria with respect to Eurasia; in all cases, surface motion resembles a pattern typical of a dense lithosphere sinking into a surrounding buoyant asthenosphere (Text S4 and Figures S8-S12). Although our models reproduce the first-order observations in the Alps and its foreland regions, modelled topography does not match the first-order observations in the Adriatic Sea (i.e., low topography with respect to the Alps). A possible reason for this mismatch stems from a lack of constraints on the configuration and nature of the crust in this region. It is also possible that the present-day deformation in the Adriatic Sea is influenced significantly by a far-field Mediterranean-scale mantle flow not included in this study (Faccenna et al., 2014; Faccenna & Becker, 2010).

Our models also fail in reproducing the coherent orogen parallel flow in the asthenosphere, which is inferred as a proxy in the SKS measurements. These discrepancies demand attention towards which additional factors could influence this behavior. Return flow from neighboring slabs in the Mediterranean could provide an alternative (e.g., Kiraly et al., 2021). Our models are spatially limited to the Alps and the Northern Apennines, and therefore we could not quantify to which degree the present-day mantle flow in the Alps can be affected by such a Mediterranean-scale return flow from the Aegean subduction in the east and the W-E directed mantle flow from the west (Faccenna & Becker, 2010).

We finally note that modelled vertical velocities in the Alps are in the same order of magnitudes as those derived from GNSS data (Figures 1 and 3). Further work is required to quantify the relative contribution from surface processes (e.g., long-term erosion, loading and unloading of the LGM ice sheets) and their coupling to the active tectonic processes investigated in this study within higher resolution models.

Acknowledgements

This work is funded by the Deutsche Forschungsgemeinschaft (DFG) through the Special Priority Program "Mountain Building Processes in Four Dimensions (4DMB)". Computations were performed on the JUWELS cluster from Jülich Supercomputing Centre (JSC) under the computing project UNEX and GAIA cluster from Johannes Gutenberg University of Mainz. Post-processing and plotting of the results was done using ParaView, GMT5, Matplotlib and Inkscape. Scientific color maps from https://www.fabiocrameri.ch/colourmaps/ were used for visualization.

Code and data sharing statement

The crustal models used can be downloaded from https://doi.org/10.5880/GFZ.4.5.2019.004 and https://gfzpublic.gfz-potsdam.de/pubman/item/item_238001. Seismic tomography models can be downloaded from http://ds.iris.edu/ds/products/emc-earthmodels/. LaMEM is an open-source code and can be downloaded from https://bitbucket.org/bkaus/lamem/src/master/. Code used for converting seismic velocities to temperatures can be downloaded from https://doi.org/10.5281/zenodo.6538257.

References

Afonso, J. C., Fernàndez, M., Ranalli, G., Griffin, W. L., & Connolly, J. A. D. (2008). Integrated geophysical-petrological modeling of the lithosphere and sublithospheric upper mantle: Methodology and applications. *Geochemistry, Geophysics, Geosystems*, *9*(5). https://doi.org/10.1029/2007GC001834Afonso, J. C., Rawlinson, N., Yang, Y., Schutt, D. L., Jones, A. G., Fullea, J., & Griffin, W. L. (2016). 3-D multiobservable probabilistic inversion for the compositional and thermal structure of the lithosphere and upper mantle: III. Thermochemical tomography in the Western-Central U.S. *Journal of Geophysical Research: Solid Earth*, *121*, 7337–7370. https://doi.org/10.1002/2016JB013049Afonso, J. C., & Zlotnik, S. (2011). The Subductability of Continental Lithosphere: The Before and After Story. In *Frontiers in Earth Sciences* (Vol. 4, Issue April). https://doi.org/10.1007/978-3-540-88558-0Amante, C., & Eakins, B. W. (2009). ETOPO1 1 Arc-Minute Global Relief Model: Procedures, Data Sources and Analysis. *NOAA Technical Memorandum NESDIS NGDC-24*. https://doi.org/10.1594/PANGAEA.769615Artemieva, I. M. (2019). Lithosphere structure in Europe from thermal isostasy. *Earth-Science Reviews*, *188*(October 2018), 454–468. https://doi.org/10.1016/j.earscirev.2018.11.004Barruol, G., Bonnin, M., Pedersen, H., Bokelmann, G. H. R., & Tiberi, C. (2011). Belt-parallel mantle flow beneath a halted continental collision: The Western Alps. *Earth and Planetary Science Letters*, *302*(3–4), 429–438. https://doi.org/10.1016/j.epsl.2010.12.040Cammarano, F., Goes, S., Vacher, P., & Giardini, D. (2003). Inferring upper-mantle temperatures from

seismic velocities. *Physics of the Earth and Planetary Interiors*, *138*(3–4), 197–222. https://doi.org/10.1016/S0031-9201(03)00156-0Chiarabba, C., Jovane, L., & DiStefano, R. (2005). A new view of Italian seismicity using 20 years of instrumental recordings. *Tectonophysics*, *395*(3–4), 251–268. https://doi.org/10.1016/j.tecto.2004.09.013Connolly, J. A. D. (2005). Computation of phase equilibria by linear programming: A tool for geodynamic modeling and its application to subduction zone decarbonation. *Earth and Planetary Science Letters*, *236*(1–2), 524–541. https://doi.org/10.1016/j.epsl.2005.04.033Connolly, J. A. D. (2009). The geodynamic equation of state: What and how. *Geochemistry, Geophysics, Geosystems*, *10*(10). https://doi.org/10.1029/2009GC002540Crameri, F., Schmeling, H., Golabek, G. J., Duretz, T., Orendt, R., Buiter, S. J. H., May, D. A., Kaus, B. J. P., Gerya, T. V., & Tackley, P. J. (2012). A comparison of numerical surface topography calculations in geodynamic modelling: An evaluation of the "sticky air" method. *Geophysical Journal International*, *189*(1), 38–54. https://doi.org/10.1111/j.1365-246X.2012.05388.xEl-Sharkawy, A., Meier, T., Lebedev, S., Behrmann, J. H., Hamada, M., Cristiano, L., Weidle, C., & Köhn, D. (2020). The Slab Puzzle of the Alpine-Mediterranean Region: Insights From a New, High-Resolution, Shear Wave Velocity Model of the Upper Mantle. *Geochemistry, Geophysics, Geosystems*, *21*(8). https://doi.org/10.1029/2020GC008993Faccenna, C., & Becker, T. W. (2010). Shaping mobile belts by small-scale convection. *Nature*, *465*(7298), 602–605. https://doi.org/10.1038/nature09064Faccenna, C., Becker, T. W., Auer, L., Billi, A., Boschi, L., Brun, J. P., Capitanio, F. A., Funiciello, F., Horvàth, F., Jolivet, L., Piromallo, C., Royden, L., Rossetti, F., & Serpelloni, E. (2014). Mantle dynamics in the Mediterranean. *Reviews of Geophysics*, *52*, 283–332. https://doi.org/10.1002/2013RG000444Fichtner, A., Trampert, J., Cupillard, P., Saygin, E., Taymaz, T., Capdeville, Y., & Villaseñor, A. (2013). Multiscale full waveform inversion. *Geophysical Journal International*, *194*(1), 534–556. https://doi.org/10.1093/gji/ggt118Fichtner, A., van Herwaarden, D. P., Afanasiev, M., Simutė, S., Krischer, L., Çubuk-Sabuncu, Y., Taymaz, T., Colli, L., Saygin, E., Villaseñor, A., Trampert, J., Cupillard, P., Bunge, H. P., & Igel, H. (2018). The Collaborative Seismic Earth Model: Generation 1. *Geophysical Research Letters*, *45*(9), 4007–4016. https://doi.org/10.1029/2018GL077338Foulger, G. R., Panza, G. F., Artemieva, I. M., Bastow, I. D., Cammarano, F., Evans, J. R., Hamilton, W. B., Julian, B. R., Lustrino, M., Thybo, H., & Yanovskaya, T. B. (2013). Caveats on tomographic images. *Terra Nova*, *25*(4), 259–281. https://doi.org/10.1111/ter.12041Fox, M., Herman, F., Kissling, E., & Willett, S. D. (2015). Rapid exhumation in the Western Alps driven by slab detachment and glacial erosion. *Geology*, *43*(5), 379–382. https://doi.org/10.1130/G36411.1Goes, S., Govers, R., & Vacher, P. (2000). Shallow mantle temperatures under Europe from P and S wave tomography. *Journal of Geophysical Research: Solid Earth*, *105*(B5), 11153–11169. https://doi.org/10.1029/1999JB900300Griffin, W. L., O'Reilly, S. Y., Afonso, J. C., & Begg, G. C. (2009). The composition and evolution of lithospheric

mantle: A re-evaluation and its tectonic implications. *Journal of Petrology*, *50*(7), 1185–1204. https://doi.org/10.1093/petrology/egn033Hammond, W. C., & Humphreys, E. D. (2000). Upper mantle seismic wave attenuation: Effects of realistic partial melt distribution. *Journal of Geophysical Research: Solid Earth*, *105*(B5), 10987–10999. https://doi.org/10.1029/2000jb900042Handy, M. R., Schmid, S. M., Paffrath, M., & Friederich, W. (2021). Orogenic lithosphere and slabs in the greater Alpine area - Interpretations based on teleseismic P-wave tomography. *Solid Earth*, *12*(11), 2633–2669. https://doi.org/10.5194/se-12-2633-2021Hein, G., Kolinsky, P., Bianchi, I., & Bokelmann, G. (2021). Shear wave splitting in the Alpine region. *Geophysical Journal International*, *227*(3), 1996–2015. https://doi.org/10.1093/gji/ggab305Heit, B., Mancilla, F. de L., Yuan, X., Morales, J., Stich, D., Martín, R., & Molina-Aguilera, A. (2017). Tearing of the mantle lithosphere along the intermediate-depth seismicity zone beneath the Gibraltar Arc: The onset of lithospheric delamination. *Geophysical Research Letters*, *44*(9), 4027–4035. https://doi.org/10.1002/2017GL073358Hirschmann, M. M. (2000). *Mantle solidus: Experimental constraints and the effects of peridotite composition*. *1*, 2000GC000070.Holland, T. J. B., & Powell, R. (1998). An internally consistent thermodynamic data set for phases of petrological interest. *Journal of Metamorphic Geology*, *16*(3), 309–343. https://doi.org/10.1111/j.1525-1314.1998.00140.xJackson, I., & Faul, U. H. (2010). Grainsize-sensitive viscoelastic relaxation in olivine: Towards a robust laboratory-based model for seismological application. *Physics of the Earth and Planetary Interiors*, *183*, 151–163. https://doi.org/10.1016/j.pepi.2010.09.005Kästle, E. D., Rosenberg, C., Boschi, L., Bellahsen, N., Meier, T., & El-Sharkawy, A. (2020). Slab break-offs in the Alpine subduction zone. *International Journal of Earth Sciences*, *109*(2), 587–603. https://doi.org/10.1007/s00531-020-01821-zKaus, B. J. P., Mühlhaus, H., & May, D. A. (2010). A stabilization algorithm for geodynamic numerical simulations with a free surface. *Physics of the Earth and Planetary Interiors*, *181*(1–2), 12–20. https://doi.org/10.1016/j.pepi.2010.04.007Kennett, B. L. N., & Engdahl, E. R. (1991). Traveltimes for global earthquake location and phase identification. *Geophysical Journal International*, *105*(2), 429–465.Kiraly, A., Funiciello, F., Capitanio, F. A., & Faccenna, C. (2021). *Dynamic interactions between subduction zones*. *202*(April). https://doi.org/10.1016/j.gloplacha.2021.103501Kissling, E., & Schlunegger, F. (2018). *Rollback Orogeny Model for the Evolution of the Swiss Alps*. *37*, 1097–1115. https://doi.org/10.1002/2017TC004762Kumar, A., Fernàndez, M., Jimenez-Munt, I., Torne, M., Vergés, J., & Afonso, J. C. (2020). LitMod2D_2.0: An improved integrated geophysical-petrological modeling tool for the physical interpretation of upper mantle anomalies. *Geochemistry, Geophysics, Geosystems*, *0*, 1–19. https://doi.org/10.1029/2019gc008777Lippitsch, R. (2003). Upper mantle structure beneath the Alpine orogen from high-resolution teleseismic tomography. *Journal of Geophysical Research*, *108*(B8), 1–15. https://doi.org/10.1029/2002jb002016Mancilla, F. de L., Booth-Rea, G., Stich, D., Pérez-Peña, J. V., Morales, J., Azañón, J. M., Martin, R., & Giaconia, F. (2015). Slab rupture and delamination under the Betics

and Rif constrained from receiver functions. *Tectonophysics*, *663*, 225–237. https://doi.org/10.1016/j.tecto.2015.06.028Mark R. Handy, Stefan M. Schmid, Marcel Paffrath, W. F. and the A. W. G. (2021). European tectosphere and slabs beneath the greater Alpine area - Interpretation of mantle structure in the Alps-Apennines-Pannonian region from teleseismic Vp studies. *Solid Earth Discussions*, *May*, 6.Mey, J., Scherler, D., Wickert, A. D., Egholm, D. L., Tesauro, M., Schildgen, T. F., & Strecker, M. R. (2016). Glacial isostatic uplift of the European Alps. *Nature Communications*, *7*, 1–10. https://doi.org/10.1038/ncomms13382Paffrath, M., Friederich, W., Schmid, S. M., & Handy, M. R. (2021). Imaging structure and geometry of slabs in the greater Alpine area - A P-wave travel-time tomography using AlpArray Seismic Network data. *Solid Earth*, *12*(11), 2671–2702. https://doi.org/10.5194/se-12-2671-2021Priestley, K., & McKenzie, D. (2006). The thermal structure of the lithosphere from shear wave velocities. *Earth and Planetary Science Letters*, *244*(1–2), 285–301. https://doi.org/10.1016/j.epsl.2006.01.008Schaeffer, A. J., & Lebedev, S. (2013). Global shear speed structure of the upper mantle and transition zone. *Geophysical Journal International*, *194*(1), 417–449. https://doi.org/10.1093/gji/ggt095Serpelloni, E., Vannucci, G., Anderlini, L., & Bennett, R. A. (2016). Kinematics, seismotectonics and seismic potential of the eastern sector of the European Alps from GPS and seismic deformation data. *Tectonophysics*, *688*, 157–181. https://doi.org/10.1016/j.tecto.2016.09.026Singer, J., Diehl, T., Husen, S., Kissling, E., & Duretz, T. (2014). Alpine lithosphere slab rollback causing lower crustal seismicity in northern foreland. *Earth and Planetary Science Letters*, *397*, 42–56. https://doi.org/10.1016/j.epsl.2014.04.002Spooner, C., Scheck-Wenderoth, M., Cacace, M., & Anikiev, D. (2022). How Alpine seismicity relates to lithospheric strength. *International Journal of Earth Sciences*, *April*, 1–24. https://doi.org/10.1007/s00531-022-02174-5Spooner, C., Scheck-Wenderoth, M., Cacace, M., Götze, H. J., & Luijendijk, E. (2020). The 3D thermal field across the Alpine orogen and its forelands and the relation to seismicity. *Global and Planetary Change*, *193*(July), 103288. https://doi.org/10.1016/j.gloplacha.2020.103288Spooner, C., Scheck-Wenderoth, M., Götze, H.-J., Ebbing, J., & Hetényi, G. (2019). Density distribution across the Alpine lithosphere constrained by 3D gravity modelling and relation to seismicity and deformation. *Solid Earth Discussions*, 1–26. https://doi.org/10.5194/se-2019-115Sternai, P., Sue, C., Husson, L., Serpelloni, E., Becker, T. W., Willett, S. D., Faccenna, C., Di Giulio, A., Spada, G., Jolivet, L., Valla, P., Petit, C., Nocquet, J. M., Walpersdorf, A., & Castelltort, S. (2019). Present-day uplift of the European Alps: Evaluating mechanisms and models of their relative contributions. *Earth-Science Reviews*, *190*(December 2018), 589–604. https://doi.org/10.1016/j.earscirev.2019.01.005Tesauro, M., Kaban, M. K., & Cloetingh, S. A. P. L. (2008). EuCRUST-07: A new reference model for the European crust. *Geophysical Research Letters*, *35*(5), 3–7. https://doi.org/10.1029/2007GL032244Wenzel, F., Sperner, B., Lorenz, F., & Mocanu, V. (2002). *Geodynamics , tomographic images and seismicity of the Vrancea region (SE-Carpathians , Romania).* 95–104.Winter, J. D. (2010).

An Introduction to Igneous and Metamorphic Petrology. Prentice Hall, New York.Workman, R. K., & Hart, S. R. (2005). Major and trace element composition of the depleted MORB mantle (DMM). *Earth and Planetary Science Letters*, *231*(1–2), 53–72. https://doi.org/10.1016/j.epsl.2004.12.005Zhu, H., Bozdăg, E., & Tromp, J. (2015). Seismic structure of the European upper mantle based on adjoint tomography. *Geophysical Journal International*, *201*(1), 18–52. https://doi.org/10.1093/gji/ggu492